Inverse Method to Obtain Blocked Forces of Vibrating Sound Sources in Buildings

Christoph Höller [*], Barry M. Gibbs
Acoustics Research Unit, University of Liverpool, Liverpool L69 7ZN, UK.
*Now at National Research Council Canada, Ottawa, Ontario K1A 0R6

Summary
Vibrating sources, such as building service equipment, are major contributors to noise in buildings. In order to predict and subsequently reduce the sound pressure levels generated by these devices, it is necessary to first predict the total vibrational power injected by them into the supporting building structure. Whilst simplified methods are available for calculation of the total power through all contacts, it would be beneficial to have more detailed knowledge of the dominant contact powers. For sources on low-mobility building elements, the contact powers are determined by the blocked force, along with the real part of the receiver mobility at each contact. This paper describes a novel inverse method to obtain the blocked forces at each contact. The method employs an instrumented reception plate, which is numerically modelled to allow optimum accelerometer positions to be selected, for any source and any location. The underlying theory and measurement procedure are described, and experimental validations are presented.

PACS no. 43.40.Yq, 43.40.Sk

1. Introduction

1.1.Structure-borne sound sources

In order to predict and subsequently reduce the noise levels generated by vibrating sources in buildings, such as services equipment, it is necessary to first estimate the total vibrational power injected by the sources into the supporting building elements. Whilst simplified indirect methods are available to obtain the total power [1], it would be useful to have detailed knowledge of the powers at each contact to identify the dominant powers for control.

This paper considers the special but common condition of high-mobility sources connected to low-mobility building elements. In this situation, the contact powers are determined by the blocked force and real part of the receiver mobility at each contact. Blocked forces are the forces at the terminals of the source when the velocity at the terminals is zero. Direct measurement of blocked forces can be problematical, both in ensuring that the test receiver structure is inert and in installing force transducers between source and receiver at all contacts, without adversely affecting the mount conditions [2].

The approximate method for the total power, described in EN 15657-1 [1], is known as the reception plate method (RPM). The source of interest is placed on a low-mobility plate, in the Standard, a resiliently supported 100mm thick concrete plate, and the source is operated under otherwise normal conditions. The total power from the source, through all contacts with the reception plate, equals the plate power, which is calculated from the plate parameters as [3]

$$P_{source} = P_{plate} = \omega \eta m \left\langle v^2 \right\rangle \qquad (1)$$

The mean-square plate velocity $\left\langle v^2 \right\rangle$ is recorded using accelerometers distributed over the plate surface. The loss factor η of the plate of mass m is obtained from the structural reverberation times of the plate. Implicit is the assumption that the plate power is wholly determined by the plate bending energy and total loss factor. Therefore, the source's contribution to the plate bending energy determines the source total power.

In many cases, knowledge of the total power is sufficient for the prediction of the resultant structure-borne sound pressure levels when the source is installed in a building [4]. However, for sources with significant differences in the mount point conditions, due to differences in vibration levels and mobility, more detailed analysis and design is required, in particular, the hierarchy of blocked forces is desirable. The advantage of using blocked forces instead of contact forces is that the former are independent of installation conditions [2].

1.2. Inverse force determination

The determination of forces, and also moments, plays an important role in many applications in noise control engineering. For instance, operational forces and moments are required as input data for Transfer Path Analysis (TPA) methods in the automotive and aerospace industries [5-7], and there is a substantial body of work on inverse force determination [8-11]. Inverse methods have been developed because direct measurements of forces and moments pose greater challenges than the measurements of linear or angular accelerations or velocities. Transducers must be inserted between the source and receiver, likely altering the transmission paths and the transmitted structure-borne power. With regards to moments, direct measurement is not possible at present. To circumvent these problems, inverse methods have been developed, for example the mount stiffness method [12], transmissibility methods [13], and the matrix inversion method, which is considered in this paper. Whilst moments cannot be neglected a priori, in building situations, the forces perpendicular to the receiver structure are generally dominant [14, 15]. In this discussion, forces perpendicular to the receiver structure only are considered.

The contact force and the contact velocity are linked by the receiver point mobility: $v_c = Y_r F_c$. If there is more than one contact, the forces and velocities are vectors, and the receiver mobility is a matrix:

$$\mathbf{v_c} = \mathbf{Y_r F_c} \qquad (2)$$

For velocities $\mathbf{v_r}$ on the receiver structure remote from the contacts, $\mathbf{Y_r}$ is a transfer mobility matrix, see Figure 1, which is also termed the FRF matrix.

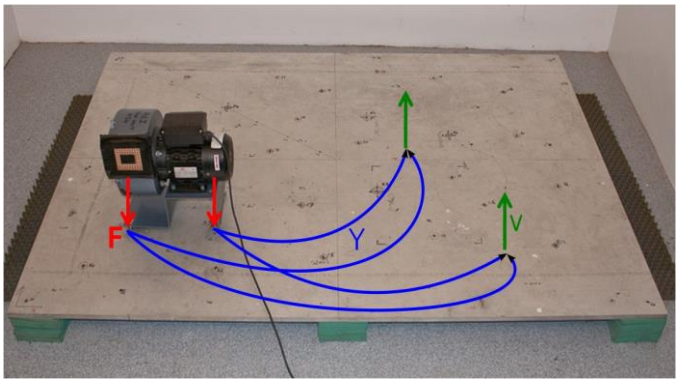

Figure 1. Fan unit connected to reception plate, showing vibration responses at the interface and typical remote positions

To obtain the contact forces, the matrix is inverted:

$$\mathbf{F_c} = \mathbf{Y_r}^{-1}\mathbf{v_r} \quad (3)$$

Equation 3 points to a three-step procedure for indirectly obtaining the contact forces:

1. The FRF matrix $\mathbf{Y_r}$ of the uncoupled receiver structure is measured, by applying forces at each of the contact positions one at a time, and recording the responses at all response positions.
2. The source is connected to the structure, and the velocities $\mathbf{v_r}$ at the same response positions are recorded during operation of the source.
3. The contact forces are calculated from Equation 3. The FRF matrix is inverted frequency by frequency, and multiplied with the velocity response vector.

This approach is termed the matrix inversion method, and is used where the contributions of each source of excitation and along each transmission path are analysed individually and rank-ordered [5].

There are two principal challenges in matrix inversion. The first concerns the determination of the FRF matrix $\mathbf{Y_r}$ which increases in size according to the square of the number of contact points. No forces or transmission paths may be omitted a priori, meaning all relevant matrix elements have to be determined, usually by measurement. This can result in a large measurement effort, which limits the applicability of this approach, in particular in building acoustics. The second challenge stems from the necessary inversion of the FRF matrix and the problems posed by ill condition.

The contact forces obtained using Equation 3 are specific to the installed condition, i.e. to the source-receiver dynamic interaction, often expressed as source-receiver mobility ratio. If the receiver structure is modified or the source is moved, a new calculation of the contact forces is required, which entails a new set of measurements of the altered FRF matrix. To overcome this limitation, Moorhouse, Elliott and Evans [2] propose that instead of inverting the FRF matrix of the uncoupled receiver mobilities, $\mathbf{Y_r}$, the FRF matrix of the coupled mobilities, $\mathbf{Y_c}$ is inverted:

$$\mathbf{F_b} = \mathbf{Y_c}^{-1}\mathbf{v_r} \quad (4)$$

Equation 4 yields the blocked forces, which are independent of the receiver structure. It requires the determination of the coupled transfer mobility matrix and thus access to the source-receiver interface to attach accelerometers. This is similar to the determination of the uncoupled mobility matrix. Höller and Gibbs propose a further development, which does not require access to the source-receiver interface [16]. Equation 4 has been used in several studies, but common to all are problems associated with matrix inversion and the challenge of obtaining all necessary mobility terms.

If however, the mobility matrix $\mathbf{Y_R}$ can be calculated instead of measured, then economies of time and effort result. For simple receiver structures, finite element methods or analytical methods can be employed. The reception plate method uses a rectangular plate with free boundary conditions. The reception plate is designed for ease of set-up and measurement. It also resembles the plate-like receivers commonly found in buildings. Calculating the mobility matrix also avoids errors due to low-quality data or measurement errors, and it further allows the investigation of methods to improve the accuracy of the matrix inversion. For example, a numerical model of the receiver structure allows the determination of the optimum plate response positions.

2. Inverse method for determining blocked forces

The contact forces $\mathbf{F_c}$ can be expressed as a function of blocked forces $\mathbf{F_b}$ and source and receiver mobility $\mathbf{Y_s}$ and $\mathbf{Y_r}$, respectively:

$$\mathbf{F_c} = (\mathbf{Y_s} + \mathbf{Y_r})^{-1}\,\mathbf{Y_s}\mathbf{F_b} \quad (5)$$

Again, if the source mobility is significantly higher than the receiver mobility, then the contact forces approximate the blocked forces:

$$\mathbf{F_c} \approx \mathbf{F_b} \text{ for } \mathbf{Y_s} >> \mathbf{Y_r} \quad (6)$$

A ratio of source mobility to receiver mobility of 10 is appropriate, which corresponds to a level difference of 10 dB (using the 10log convention). The 100mm thick concrete plate, specified in the Standard EN15657-1 [1], fulfils the requirement for most vibrating sources in buildings.

The measurement procedure for the inverse determination of blocked forces is as follows:

1. The geometrical distance between source contacts is measured, and the source placed on the plate at a position that ensures that the source contacts are not at nodal lines.
2. Based on the numerical model of the plate, suitable response positions can be determined [17].
3. The FRF matrix is calculated, using a numerical model of the receiver.
4. Velocity spectra are measured at the response positions during operation of the source. This is the only required measurement.

5. From the calculated FRF matrix and the measured velocity responses, the contact forces are determined.

The key to the proposed measurement procedure is the analytical or numerical model of the receiver plate.

3. Models of FFFF plate

In modelling the free plate, the point and transfer mobilities are expressed in terms of modal summations, with mode shapes calculated either analytically or numerically (e.g. using FE).

Analytical and numerical models of plates have been studied extensively [18, 19]. Leissa [18] gives a compendium of formulations for plates with different boundary conditions and aspect ratios. The following calculations of point and transfer mobilities of thin rectangular plates are based on methods described in [20], which in turn are based on [19] and [21]. The point and transfer mobilities for bending vibration of thin finite plates can be expressed in terms of a modal summation. A rectangular plate is excited by a force at position (x_1, y_1), and the linear or angular response velocity determined at position (x_2, y_2). The point and transfer mobilities for force excitation are given as:

$$Y_{v_z F_z}(\omega) = j\omega \sum_{m=1}^{\infty}\sum_{n=1}^{\infty} \frac{\psi_{mn}(x_2, y_2)\,\psi_{mn}(x_1, y_1)}{\rho h l_x l_y \left[\omega_{mn}^2 (1 + j\eta) - \omega^2\right]} \qquad (7)$$

ψ_{mn} is the (m,n)th bending mode shape, ω_{mn} is the associated eigenfrequency, h, l_x and l_y are the dimensions of the plate, ρ is the material density, and η is the total loss factor. The upper frequency limit of the sum must be higher than, typically more than twice, the upper frequency of the range of interest.

3.1. Analytical model using beam functions

The plate mode shapes can be calculated as products of the beam mode shapes φ_m and φ_n:

$$\psi_{mn}(x,y) = \varphi_m(x)\varphi_n(y) \qquad (8)$$

Equations for the eigen-frequencies and beam modes for the most common boundary conditions are provided in [20]. The first two modes represent whole-body movement (even and rocking mode), while higher modes represent bending motion. The eigen-frequencies of rectangular plates are given as [21]:

$$\omega_{mn} = \sqrt{\frac{Eh^2}{12\rho(1-\nu^2)}}\left(\frac{\pi}{l_x}\right)^2 q_{mn} \qquad (9)$$

E is Young's modulus, ν is Poisson's ratio, and q_{mn} depends on the boundary conditions.

3.2. Finite element model

An alternative method of obtaining the plate mode shapes is through the use of a finite element model. In this study the mode shapes and eigen-frequencies of the free plate were evaluated in ABAQUS and exported to MATLAB for processing and plotting.

4. Experimental validation

4.1. Set-up

A reception plate of aluminium and of size 2.12m × 1.50m × 20mm (Figure 1) was supported at the corners and edges by visco-elastic pads (Getzner SyloDamp HD30). This configuration approximates free boundary conditions and provides additional damping. The plate was not according to the recommendations in the Standard EN15657-1 [1], but complied with requirements regarding dimensions, receiver mobility and loss factor.

Two sources were considered: a medium size fan unit on four mounts (Figure 1) and a test source, consisting of a small electrodynamic shaker, attached to the base of the same type of fan unit on four feet (Figure 2).

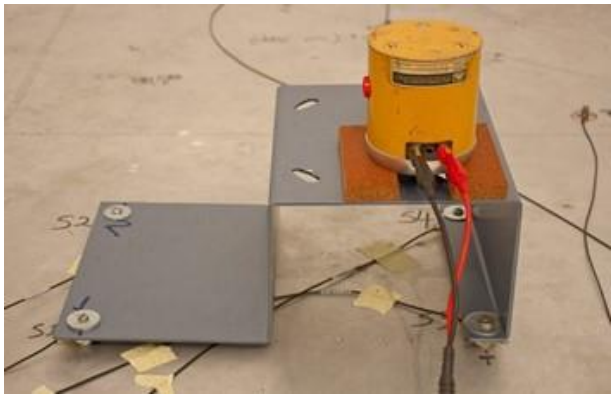

Figure 2. Test source on reception plate

The test source therefore had a similar mobility to the fan base. The shaker allowed the variation and control of the broadband excitation spectrum. The test source was mounted on the receiver plate via four force transducers, which were screwed into the source and plate. The transducers were considered to be part of the source, and directly recorded the contact forces for comparison with inverse estimates.

4.2. Measurement procedure

The response velocities, during operation of the sources, were recorded at 32 positions evenly distributed over the plate, using eight accelerometers at a time. The contact forces were recorded simultaneously using four force transducers. The measurement time was 5s, the frequency resolution Δf = 1Hz, the sampling rate f_s = 16384Hz.

Receiver point mobilities at the source contacts and transfer mobilities from the source contacts to the 32 velocity response positions (giving 128 FRFs) were measured as narrowband spectra with an impulse hammer. Five averages per FRF were recorded. A plastic hammer tip was used, ensuring a sufficient excitation force up to 2 kHz. Figure 3 shows representative point mobilities of the plate and fan unit, as narrowband and third-octave band spectra.

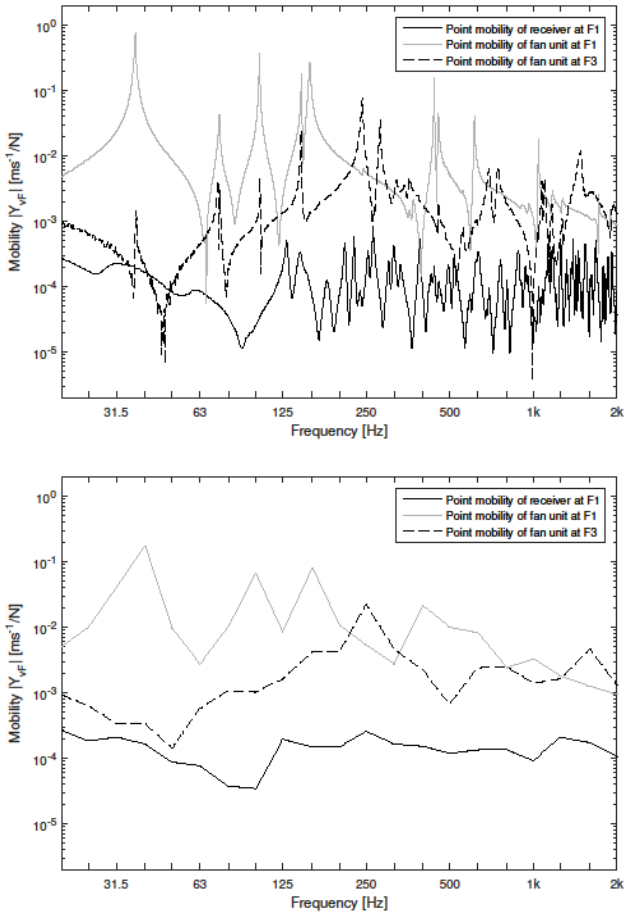

Figure 3. Test source and receiver mobility in narrow-band (upper figure) and 1/3-octave bands (lower figure).

The point mobility at F_1 is at the flexible part of the fan base, shown on the left of Figure 2. F_3 is at the stiff part of the base, shown on the right of Figure 2. In third-octave bands, the source mobility exceeds the receiver mobility by a factor of 10 (corresponding to a level difference 10 dB) above 50Hz, indicating that the high-mobility source assumption is fulfilled. The narrowband mobility spectra reveal that there are frequencies where the contact forces do not approximate the blocked forces, but these occur over small frequency ranges.

4.3. Comparison of measured and calculated FRFs

The analytical model was implemented in MATLAB and calculated and measured point mobilities were compared. The material parameters are: Young's modulus E = 70GPa, density ρ = 2700kg/m^3, Poisson's ratio ν = 0.33. The loss factor of the plate was measured in third-octave bands and values interpolated for calculation of narrowband values. Figure 4 shows the measured and calculated point mobility of the plate at position (0.325m, 0.380m), from the origin at a corner. A reduced frequency range is shown for comparison.

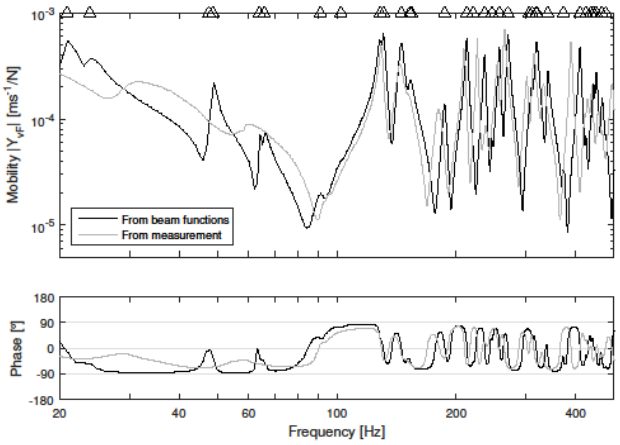

Figure 4. Measured and calculated point mobility of 20mm aluminium plate.

Below 100Hz, there are differences between calculated and measured mobility, although the frequency trends are similar. Between 100Hz and 200 Hz, there is better agreement. Above 200 Hz, there is agreement in terms of 'signature', but with shifts in the resonance frequencies. The first reason for the deviations is that the resiliently supported plate may not behave like a free plate. The resilient pads introduce some restriction on the plate movement. Secondly, the mode shapes, calculated from beam functions, are not exact for plates with free edges [21, 22].

The point mobility was also calculated using the mode shapes and eigenfrequencies obtained by the FE method, and is shown in Figure 5.

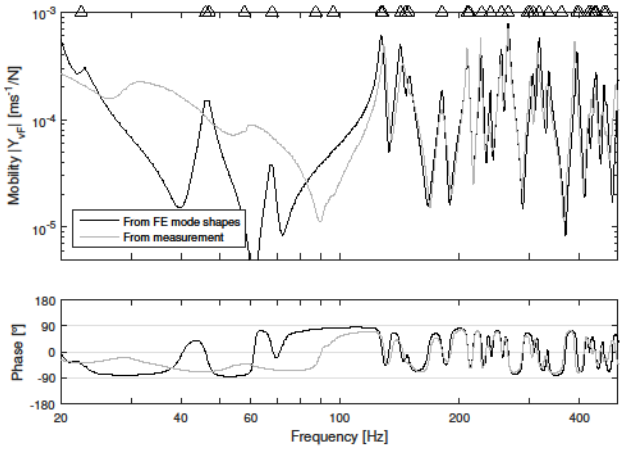

Figure 5. Measured point mobility of 20mm aluminium plate at position (0.325m, 0.380m) and calculated using FEM.

The calculations were performed with the same parameters as in the beam function model. The plate was meshed using S4R shell elements, with nodes at 25mm intervals. For a requirement of six elements per wavelength [23], the upper frequency limit is around 8.4 kHz, higher than the upper limit of 2 kHz used in the measurements. The deviations are large below 100 Hz, when compared with the deviations in the beam function model. The resonance frequencies are shifted, and the damping of the measured mobilities is higher than that of the calculated mobilities. Above 100Hz, the agreement is better than the beam function model. Occasional frequency shifts still occur, but generally the calculated eigen-frequencies approximate the measured values.

5. Inverse force determination using measured FRFs

The forces exerted on the receiver plate by the test source were calculated from measured operational velocities and measured transfer mobilities. The calculations were performed frequency by frequency, using narrowband FFT spectra. Figure 6 shows measured and calculated third-octave band force levels for the test source. The conversion of narrowband force spectra to third octave band levels was to clearly indicate differences between calculated and measured values.

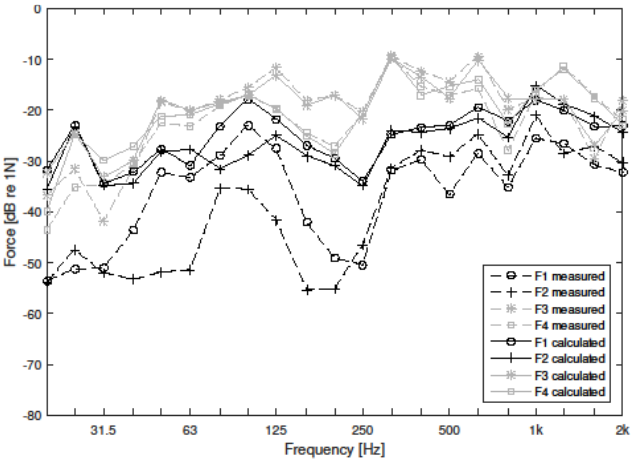

Figure 6. Measured and calculated forces.

The measured forces at the stiff end of the test source F_3 and F_4 are similar. They exceed the forces at the resilient end F_1 and F_2 by more than 10dB at frequencies below 1 kHz. Above 1 kHz, all the forces are of the same order of magnitude. The calculated high forces F_3 and F_4 generally agree with the measured forces, but the calculated low forces F_1 and F_2 are significantly over-predicted. For brevity, the following results show one dominant force F_3 and one weak force F_1.

Figure 7 shows the level differences (using 20log) between calculated and measured test source forces, and Figure 8 for the fan unit.

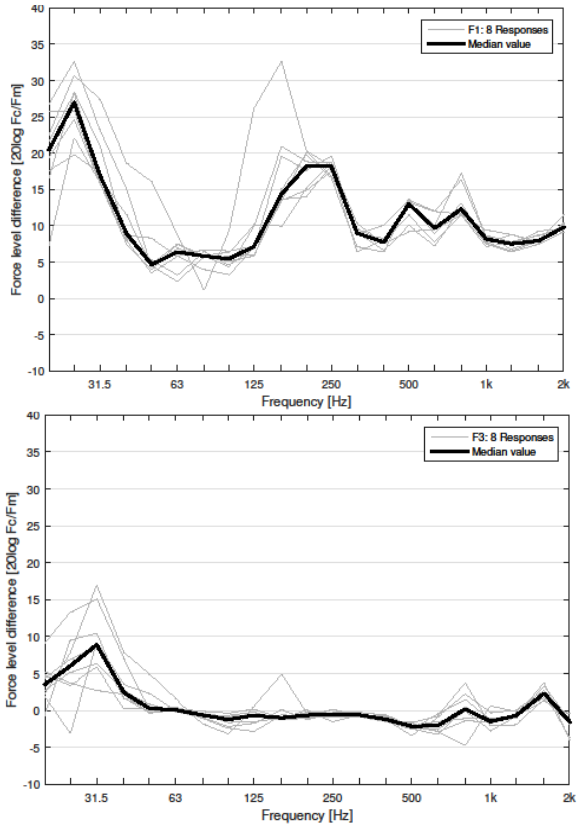

Figure 7. Level difference between estimated and measured test source forces

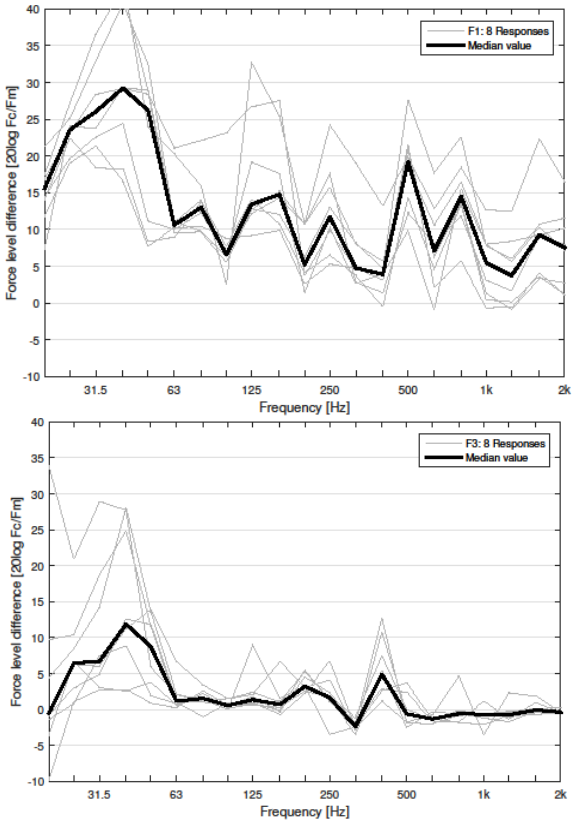

Figure 8. Level difference between estimated and measured fan forces.

Shown are median values. Positive values indicate over-estimates. For both sources and above 63 Hz, the estimated large force F_3 is within ±5 dB of the measured values. Below 63 Hz, the deviations are larger, with median errors of up to 10 dB. This may be due to the lack of contributing plate eigenmodes. The calculated eigenfrequencies indicate that only two eigenmodes contribute to the velocity responses below 50 Hz, excluding whole-body plate movement.

The low force F_1 is over-estimated, with low frequency bands showing up to 30dB deviations. This observation is in line with findings of others, that low forces in the presence of high forces are generally over-estimated [17].

Both high and low forces are generally over-predicted. If a single FFT line in the inversely determined narrowband force contains strong amplification due to matrix ill-conditioning, the containing third-octave band is over-estimated. Furthermore, the reference value for the level differences is the directly measured force. While the force transducers register translational motion, there may also be a rotational excitation component, which contributes to the response velocities. An inverse calculation yields a pseudo-force, representing both translational and rotational excitation components. For these reasons, the inverse method is likely to overestimate the contact forces.

5.1. Over determination

Matrix inversion potentially amplifies random errors in the measured velocity responses, resulting in large errors in the force estimates. To counter this, the use of over-determination and singular value rejection were investigated (see [17] for detailed discussions of these methods). Since both sources under test have four contacts, at least four responses were used.

Figure 9 shows the force level differences (i.e. from the estimated force normalised by the measured force) for the test source, for low force F_1, and Figure 10 for high force F_3. Results are shown as box plots within which are median values. The upper and lower edges of the box represent the 25th and 75th percentiles, respectively. The whiskers extend to extreme data points not considered outliers. Outliers are plotted individually as dots. The number of responses, i.e. accelerometers, was increased in unit steps from 4 to 7; 5 and 7 are shown for brevity.

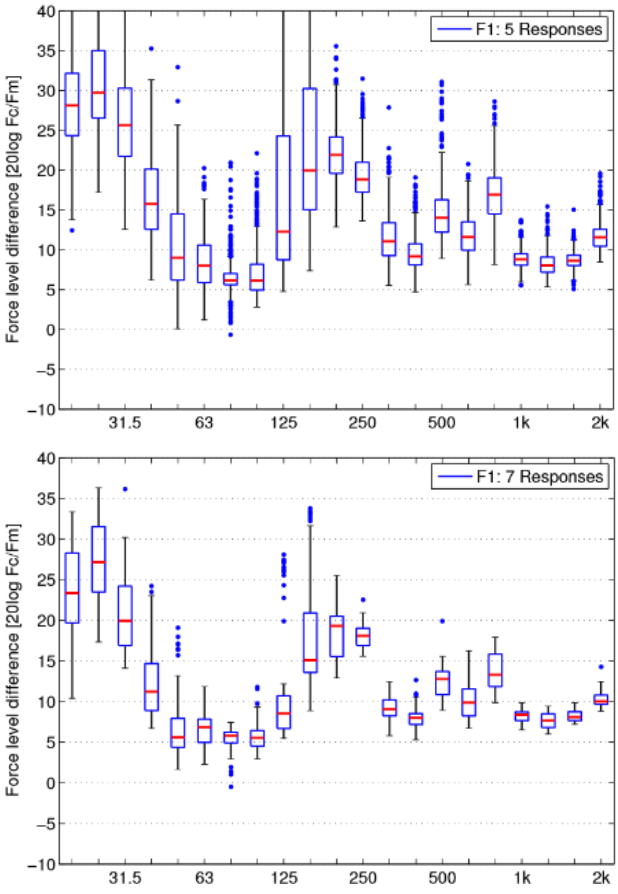

Figure 9. Level differences for F_1 of the test source for 5 (upper figure) and for 7 (lower figure) response positions.

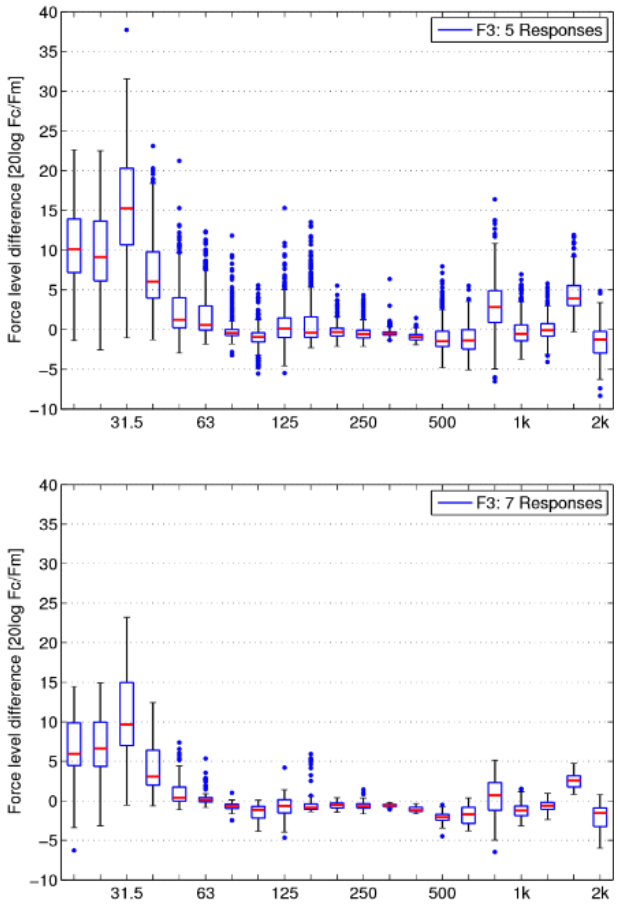

Figure 10. Level differences for F_3 of the test source for 5 (upper figure) and 7 (lower figure) response positions.

Increasing the number of responses reduces the median force level differences and also reduces the range. For the low force F_1, consider the frequencies at which maxima occur (see upper Figure 7). At 25 Hz there is little improvement in either the median or range, although there is a general improvement at other frequencies. For the high force F_3 and at 31.5 Hz, the median decreases to 9dB. At frequencies above 31.5 Hz, the median reduces to within 3 dB, accompanied by the range reducing from 8dB to 4dB. Over-determination improves results but does not significantly reduce over-estimates of low forces in the presence of high forces.

5.2. Singular value rejection

Singular value rejection (SVR) mitigates problems associated with matrix inversion. The challenge lies in selecting an appropriate rejection threshold. Four thresholds were considered: rejection of the smallest singular value; of values smaller than 1% of the highest SV; when smaller than 2%; when smaller than 10%. Each case was considered without over-determination. Figures 11 and 12 shows results for 1% and 10% SVR for low force F_1 and high force F_3, respectively.

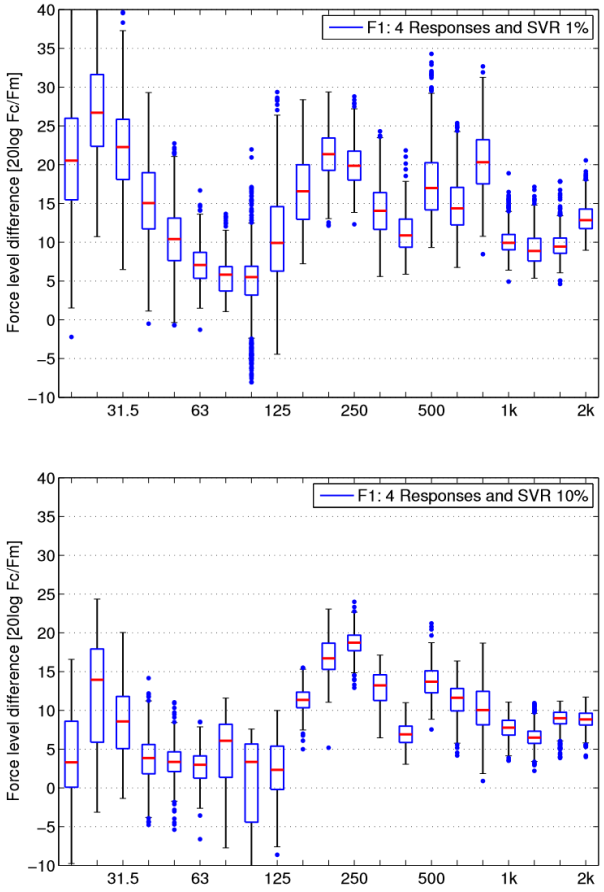

Figure 11. Level differences for F_1 for SVR of 1% (upper figure) and 10% (lower figure).

The improvement due to SVR is greater than by over-determination. The greatest improvements are achieved below 100Hz. For the low force F_1, the median at 25Hz reduces from 27dB to 14dB, for SVR 1% to 10%, respectively. For the high force F_3, the median at 31.5Hz decreases from 11dB to -2dB.

For the high force F_3 the increase in SVR leads to underestimates of -5dB. Indeed, the SVR of 1% gives acceptable estimates, most within 2dB, at frequencies above 40 Hz.

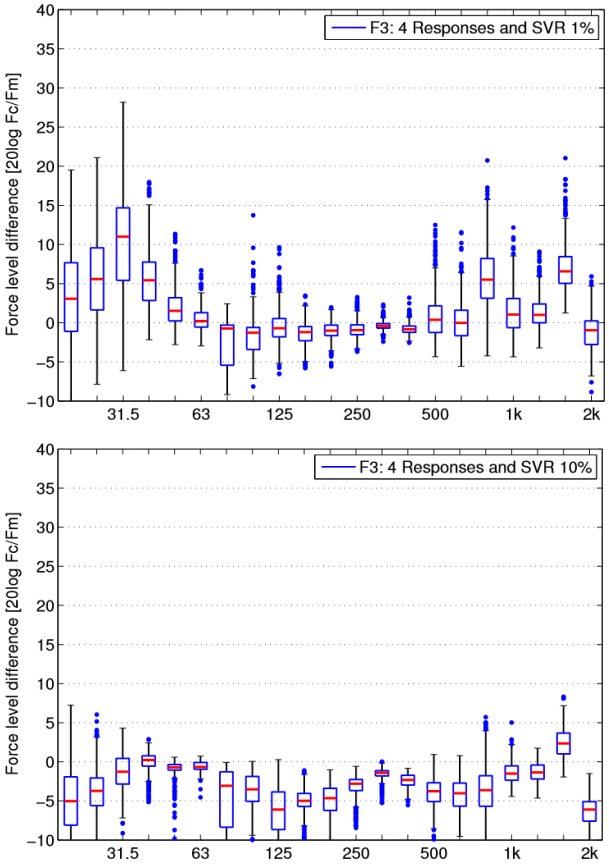

Figure 12. Level differences for F_3 for SVR of 1% (upper figure) and 10% (lower figure).

5.3. Effect of response location

The effect of velocity response (i.e. accelerometer) positions is determined by reference to the condition number of the FRF matrix (again, see [17]). Condition numbers were calculated for 560 combinations of response locations and then averaged over the frequency range 20Hz – 2 kHz, to obtain a single quantity for comparison. Whilst this can hide large discrepancies at certain frequencies, the data reduction gives an indication of favourable combinations. Inverse force determinations were performed for 4 responses and for the 20 combinations with the lowest and highest average condition numbers. The level differences are shown in Figure 13 and 14 for the low force F_1 and high force F_3, respectively.

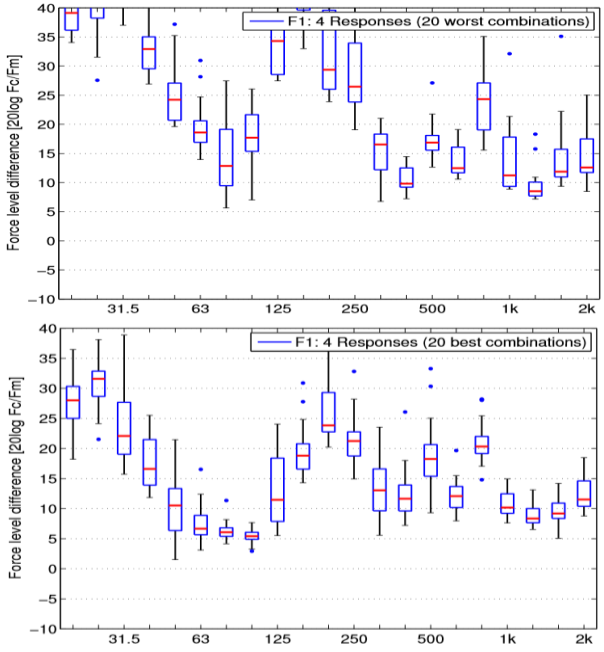

Figure 13. Level differences for F_1 for lowest (upper figure) and highest (lower figure) average condition numbers.

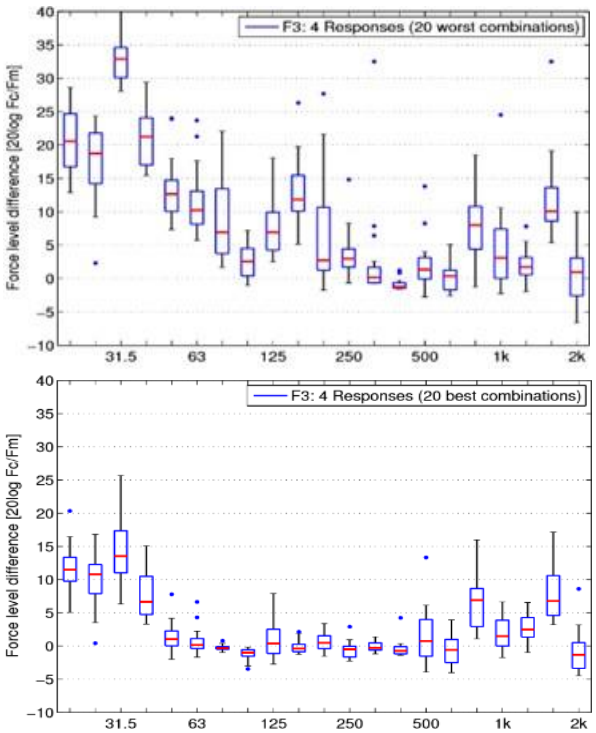

Figure 14. Level differences for F_3 for lowest (upper figure) and lowest (lower figure) average condition numbers.

In Figures 15 and 16 and concentrating on results above 50 Hz, the improvement in force estimates between bad combinations and good combinations is greater for the low force F_1 than for the high force F_3.

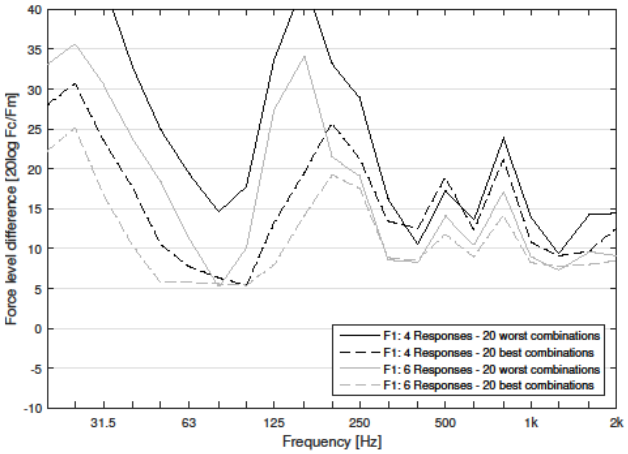

Figure 15. Deviations in F_1 estimate for: four (4R) and six (6R) responses, and 20 worst (20W) and best (20B) combinations.

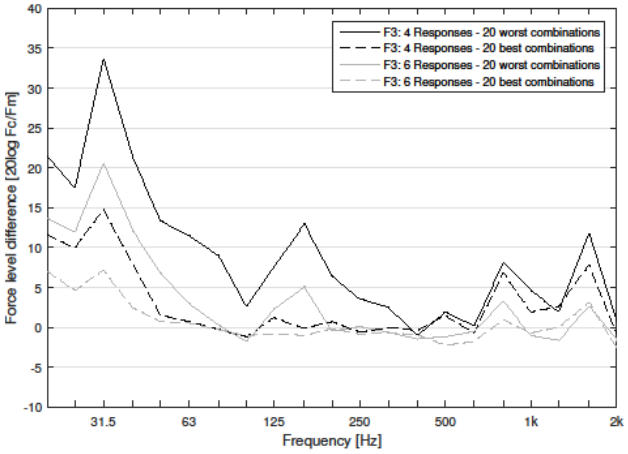

Figure 16. Deviations in F_3 estimate for: four (4R) and six responses (6R), and 20 worst (20W) and best (20B) combinations.

This points to the possibility of identifying low forces by forcing an ill condition, and thereby eliminating them from the hierarchy of forces to be included in predictions of total power and/or identified for control. This approach would be used in combination with visual inspection of the estimated forces, such as in Figure 8, where the low forces are greatly over-estimated, but still lie below the estimated high forces. The improvement from Figure 15 to Figure 16 suggests that optimization of response locations should be a primary objective for accurate force estimates.

The selection of favourable combinations of response positions poses a challenge. For the experimental study, there were 35960 combinations, when selecting four responses out of 32, and comparing the condition numbers of all these combinations requires a significant measurement and computational effort. The use of a numerical model of the receiver plate has the potential to simplify the selection process considerably.

6. Inverse force determination using calculated FRFs

The forces exerted on the receiver plate by the test source were determined inversely using calculated FRF matrices. Transfer mobilities between the four source contacts and the 32 response locations were calculated using the beam function model and the finite element model. Eigenfrequencies up to 4 kHz were considered in the modal summation. The forces then were calculated from measured operational velocities and calculated transfer mobilities. For conciseness, the test source and one high force F_3 and one low force F_1 again are considered, with the emphasis on response locations and resultant transfer mobility matrix condition number.

Figures 17 and 18 show results using beam functions and four responses. Below 100Hz, the median force level differences are significantly reduced by changing the response positions. The spread of results remains constant for F_3, but decreases for F_1. Between 100Hz and 630Hz, the medians reduce from between 26dB and 53dB to between 14dB and 43dB for F_1, and from between 9dB and 29dB to between −2dB and 16dB for F_3. Figures 19 and 20 show similar results using FEM.

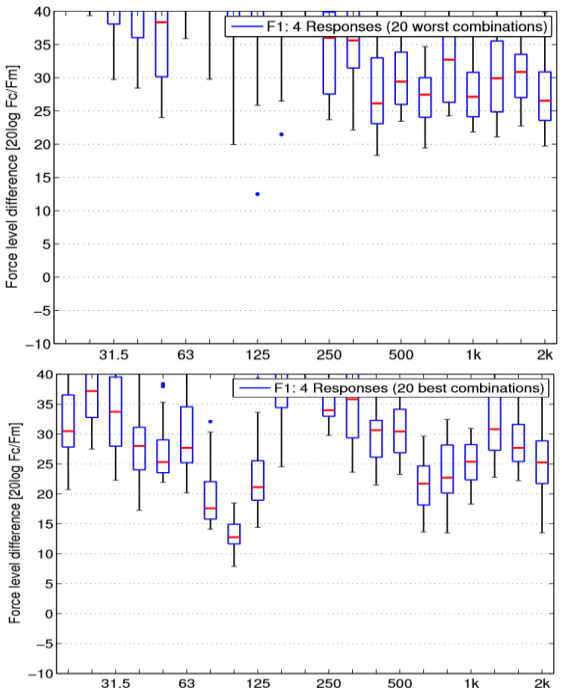

Figure 17. F_1 level difference using beam functions for the worst (upper figure) and best (lower figure) combinations.

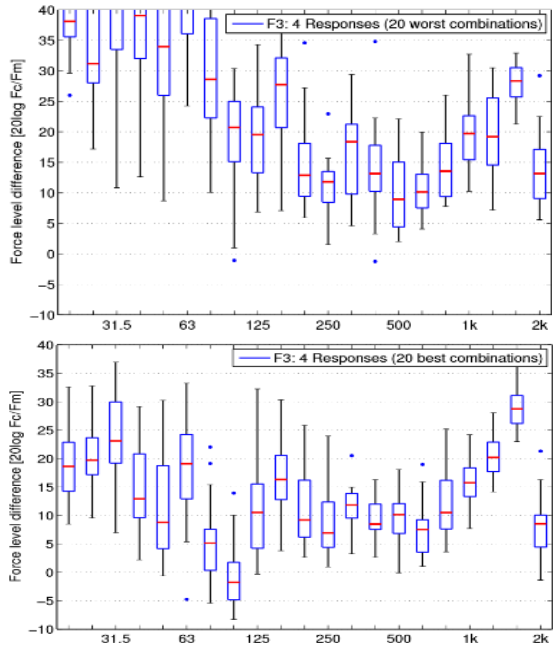

Figure 18. F_3 level difference using beam functions for the worst (upper figure) and best (lower figure) combinations.

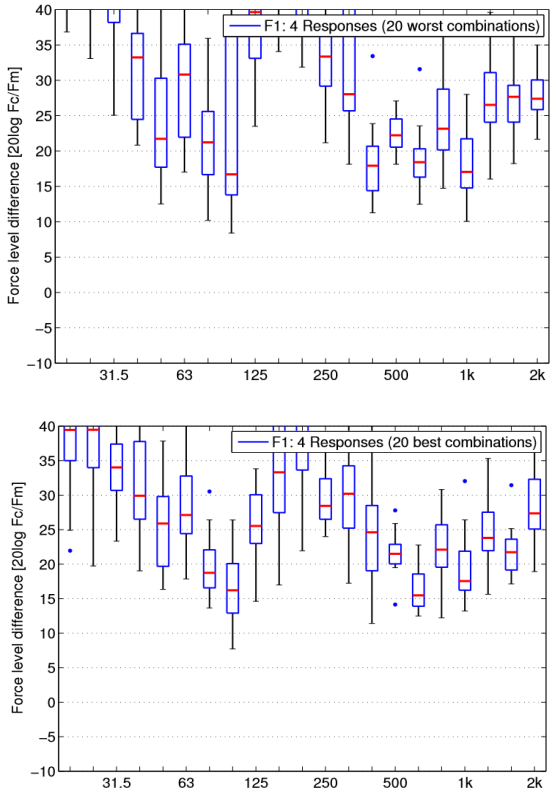

Figure 19. F_1 level difference using FEM for the worst (upper figure) and best (lower figure) combinations.

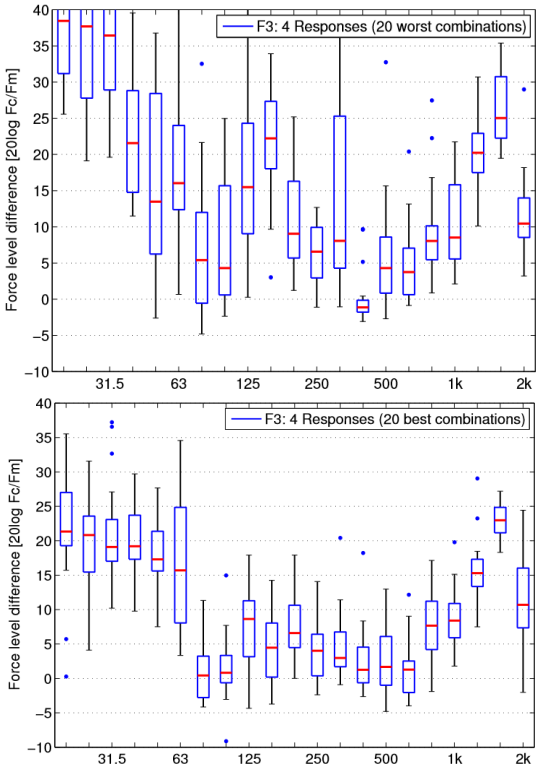

Figure 20. F_3 level difference using FEM for the worst (upper figure) and best (lower figure) combinations.

Summarizing, the use of calculated instead of measured FRFs can lead to larger errors in the force estimates. Forces obtained using beam functions exhibited larger deviations than FEM. The best results were achieved in the mid-frequency range when employing over-determination (seven responses instead of four).

When using calculated FRFs, over-determination does not entail a significant increase in measurement effort; only some additional velocity responses must be recorded. Therefore, over-determination should be used in this case. Despite the limitations of using calculated FRFs, particularly by beam functions, the method can be employed as a preliminary response optimisation, which then leads directly to the equivalent optimised measurement response locations.

7. Hybrid method using calculated and measured FRFs

Combinations of response positions with the 20 lowest and highest average condition numbers across the frequency range of interest were identified using FRFs calculated from FEM. The contact forces were then inversely determined using measured FRFs, and compared with the directly measured values. Figure 21 shows the low force F_1 level differences, for the 20 best and the 20 worst combinations. Figure 22 shows the high force F_3 level differences. Although the calculated FRFs used to determine good and bad combinations of response positions deviate from the measured FRFs used

to inversely determine the forces, the hybrid approach gives significant improvements for low force F_1. The median decreases by more than 10dB below 250Hz. For higher frequencies, the medians are approximately unchanged, but the range reduces when using combinations with a low average condition number. The improvement for the high force F_3 is between 5dB and 20dB below 250Hz, and around 2dB above 250Hz. The median for F_3, using good combinations, are within ±1.5dB between 50Hz and 630Hz, between 10dB and 15dB below 50Hz, and between 0dB and 6dB above 630Hz. This accuracy would be considered acceptable in many situations.

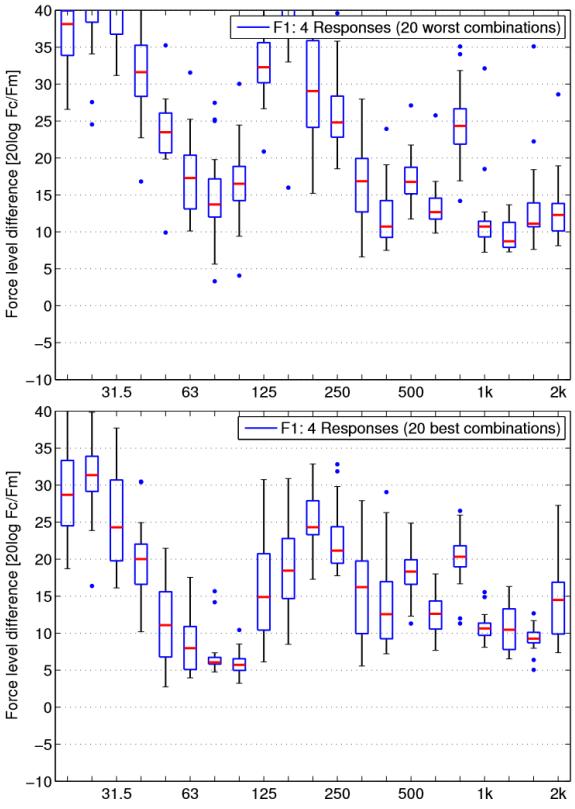

Figure 21. F_1 level differences using FEM and measured FRF for the worst (upper figure) and best (lower figure) combinations.

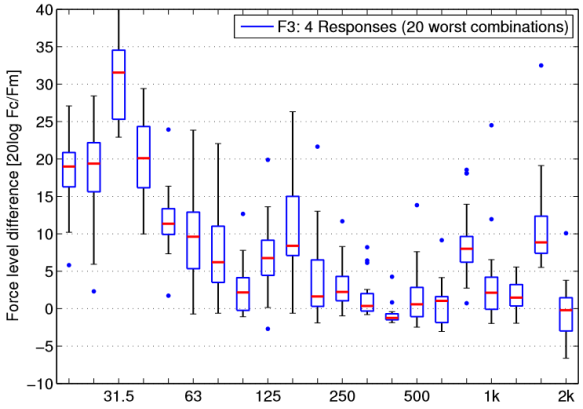

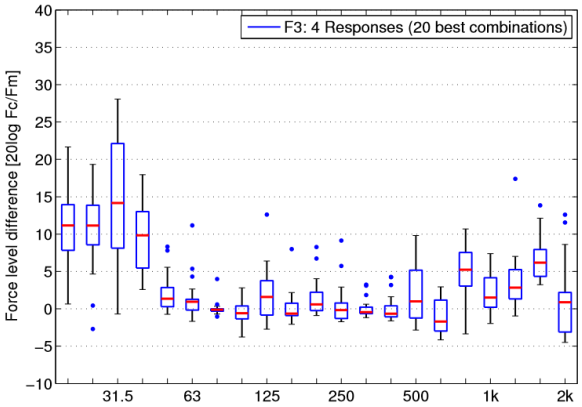

Figure 22. F_3 level differences using FEM and measured FRF for the worst (upper figure) and best (lower figure) combinations.

8. Conclusions

Inverse force determination was investigated experimentally. The forces exerted by an industrial fan unit and a test source, both on a 20mm aluminium plate, were examined. In the first stage, measured FRFs were used, together with measured operational velocities, to indirectly determine the contact forces. It was confirmed that low forces in the presence of high forces are significantly over-estimated.

Methods to improve the inverse force determination were examined. Singular value rejection is effective at low frequencies. However, the choice of an appropriate threshold is critical

Over-determination offers the best strategy. It is easy to apply, does not require monitoring of thresholds etc., and results are not degraded because of a loss of information. However, its effects are limited at low frequencies where few modes contribute.

The choice of appropriate response locations also was found to be of importance. FRFs calculated from beam functions or FE mode shapes were used together with measured operational velocities. The accuracy of the force estimates decreased significantly, due to imperfect agreement between measured and calculated FRFs. FRFs calculated from FE mode shapes gave better results than from beam function mode shapes. However, the errors in both cases were probably too large for the methods to be considered viable alternatives.

However, optimization of response positions may still be performed with calculated FRFs. Using response positions determined from calculated FRFs, inverse force determination was then performed with measured FRFs at the same positions. With this approach, the measurement effort can be reduced, while the accuracy of ordinary inverse force determination can be retained.

Acknowledgement

The authors gratefully acknowledge the financial support provided by the Engineering and Physical Sciences Research Council of the UK under grant EP/H040293/1.

References

1. EN 15657-1: 2009: Acoustic properties of building elements and of buildings – Laboratory measurement of airborne and structure-borne sound from building equipment – Part 1: Simplified cases where the equipment mobilities are much higher than the receiver mobilities, taking whirlpool baths as an example.
2. A T. Moorhouse, A. S. Elliott and T. A. Evans: In situ measurement of the blocked force of structure-borne sound sources. Journal of Sound and Vibration, 325, 679-685, 2009.
3. L. Cremer, M. Heckl and B.A.T. Petersson: Structure-borne sound, 3rd ed. Springer, Berlin Heidelberg New York, 2005.
4. EN 12354-5: 2009: Building acoustics – Estimation of acoustic performance of building from the performance of elements – Part 5: Sound levels due to service equipment.
5. LMS International: Transfer Path Analysis: The qualification and quantification of vibroacoustic transfer paths. http://www.lmsintl.com/What-is-transfer-path-analysis.
6. J. Plunt: Finding and fixing vehicle NVH problems with transfer path analysis. Sound and Vibration, 39(11), 12-16, 2005.
7. Roland Sottek and Bernard Muller-Held: Binaural transfer path analysis and synthesis (BTPA/BTPS) using sub-structuring techniques based on finite element analysis (FEA) and measurements. Proc. SAE Noise & Vibration Conference, 2007.
8. F. D. Bartlett and W. G. Flannelly: Model verification of force determination for measuring vibratory loads. Journal of the American Helicopter Society, 24(2), 10-18, 1979.
9. B. J. Dobson and E. Rider: A review of the indirect calculation of excitation forces from measured structural response data. Proc. Institution of Mechanical Engineers, Part C: Journal of Mechanical Engineering Science, 204(2), 69-75, 1990.
10. W. Hendricx: Accurate vehicle FRF measurements for indirect force determination based upon matrix inversion. Proc. 19th International Seminar on Modal Analysis (ISMA), Leuven, 1994.
11. J. W. Verheij: Inverse and reciprocity methods for machinery noise source characterization and sound path quantification Part 1: Sources. International Journal of Acoustics and Vibration, 2(1):11 20, 1997.
12. J. W. Verheij: Multi-path sound transfer from resiliently mounted shipboard machinery. PhD thesis, TU Delft, 1986.
13. P. Gajdatsy, K. Janssens, W. Desmet, and H. Van der Auweraer: Application of the transmissibility concept in transfer path analysis. Mechanical Systems and Signal Processing, 24(7), 1963-1976, 2010.
14. S. H. Yap and B. M. Gibbs: Structure-borne sound transmission from machines in buildings, Part 2: Indirect measurement of force and moment at the machine-receiver interface of a single point connected system by a reciprocal method. Journal of Sound and Vibration, 222(1), 99-113, 1999.
15. J. Scheck and B.M. Gibbs: Impacted lightweight stairs as structure-borne sound sources, Applied Acoustics 90, 9-20, 2015.
16. C. Hoeller and B.M. Gibbs: Indirect determination of the mobility of structure-borne sound sources, J. sound and Vibration 344, 38-56, 2015.
17. A. N. Thite and D. J. Thompson. The quantification of structure-borne transmission paths by inverse methods. Part 1: Improved singular value rejection methods. J. Sound and vibration 264, 411-431, 2003.
18. W. Leissa: The free vibration of rectangular plates. Journal of Sound and Vibration, 31(3), 257-293, 1973.
19. W. Soedel: Vibration of Shells and Plates. Marcel Dekker Inc., 2nd edition, 1993.
20. P. Gardonio and M. J. Brennan: Advanced Applications in Acoustics, Noise and Vibration, chapter 9: Mobility and impedance methods in structural dynamics, pages 389 447. Taylor & Francis, 2004.
21. G. B. Warburton: Vibration of rectangular plates. Proc. of the Institution of Mechanical Engineers, volume 168, pages 371 384, 1954.
22. S. F. Bassily and S. M. Dickinson: On the use of beam functions for problems of plates involving free edges. Journal of Applied Mechanics, 42(4), 858-864, 1975.
23. Carl Hopkins: Sound Insulation. Elsevier, 1st edition, 2007.